Control Strategy for Improved Dynamic Performance of Variable-Speed Drives With Modular Multilevel Converter

Jae-Jung Jung, *Student Member, IEEE*, Hak-Jun Lee, *Student Member, IEEE*, and Seung-Ki Sul, *Fellow, IEEE*

***Abstract*— This paper presents a control scheme for the modular multilevel converter (MMC) to drive a variable-speed ac machine, especially focusing on improving dynamic performance. Theoretically, the energy balance in the MMC cell capacitors is prone to be unstable at start-up and low-frequency operations. In addition, the MMC topology essentially requires advanced control strategies to balance energy and suppress the voltage pulsation of each cell capacitor. This paper proposes a control strategy for the robust dynamic response of MMC even at zero output frequency employing leg offset voltage injection. The leg offset voltage for balancing the arm energy is produced by direct calculation without the circulating current control loop controller. Thanks to the highly dynamic leg offset voltage from direct calculation and not conventional circulating current controller, the dynamic performance of an MMC at low speeds has conspicuously improved. The ac machine has been driven from standstill to rated speed without excessive cell capacitor voltage ripples utilizing this proposed strategy. The simulation and experimental results verify that stable operation is guaranteed down to <2% of the rated speed under 40% step load torque disturbance.**

***Index Terms*— Arm energy balancing, dynamic performance, inner circulating current, modular multilevel converter (MMC), motor drive.**

NOMENCLATURE

Superscript '$*$'	Reference value.
Superscript '$\sim$'	Low-frequency component.
Superscript '$\wedge$'	High-frequency component.
x-phase	Representation of one of the u, v, or w phases.
v_{xo}	Leg offset voltage of x-phase leg.
v_{sn}	Common mode voltage.
i_{xo}	Circulating current of x-phase leg.
ω_{s}	Three-phase output frequency.
R	Resistance of arm inductor.
L	Inductance of arm inductor.
C_{cell}	Capacitance of dc capacitor in a submodule cell.
E_{xP}	Upper arm energy in x-phase leg.
E_{xN}	Lower arm energy in x-phase leg.
v_{xPi}^{C}	ith cell capacitor voltage inupper arm in x-phase.
v_{xNi}^{C}	ith cell capacitor voltagein lower arm in x-phase.

Manuscript received September 1, 2013; revised December 18, 2013, February 19, 2014, and April 21, 2014; accepted April 22, 2014. Date of publication May 14, 2014; date of current version April 30, 2015. Recommended for publication by Associate Editor Joseph O. Ojo.

J.-J. Jung and S.-K. Sul are with the School of Electric and Computer Engineering, Seoul National University, Seoul 151-742, Korea (e-mail: jaejung.jung@eepel.snu.ac.kr).

H.-J. Lee is with the Corporate Technology Research and Development Center, LSIS, Anyang-si 431-080, Korea (e-mail: hjlee@eepel.snu.ac.kr).

Color versions of one or more of the figures in this paper are available online at http://ieeexplore.ieee.org.

Digital Object Identifier 10.1109/JESTPE.2014.2323955

I. INTRODUCTION

A MODULAR multilevel converter (MMC) with focus on high-power medium voltage ac motor drives is presented [1]–[10]. The use of an MMC makes it possible to save bulky reactive components in a medium-voltage motor drive application, such as a line-transformer, harmonic filter, and dc-link reactor. Compared with conventional medium voltage source converters, the MMC has a modular structure made up of identical converter cells. Because it can easily provide higher number of voltage level for medium voltage applications, the quality of the output voltage waveform is better. In addition, because of the modular structure it has advantages, such as easy maintenance and assembly.

Fig. 1 shows the circuit configuration of an MMC. This topology needs to be controlled by extra balancing strategies. As shown in Fig. 1, since the upper and lower arm currents flow through cells in each arm, the corresponding arm currents cause fundamental periodic pulsations of cell capacitor voltages. The voltage pulsation of each cell's capacitor is mostly affected by the output phase current and output frequency. Theoretically, the magnitude of the cell voltage fluctuation is proportional to magnitude of the output phase current and inversely proportional to operating frequency [6]. For this reason, special effort is demanded to drive the ac machine through MMC, which requires considerable starting torque and low-speed steady state operation. In recent studies of [7]–[9] and [16], the principles and algorithms for ac motor drives with the MMC have been introduced. However, they did not address the actual control strategies, such as changing output frequency, including standstill and coveringload torque disturbance.

The energy balancing control is one of the main issues of an MMC system. In many literatures [6]–[10], the energy balancing controls of an MMC that uses circulating current control and modulation scheme have been introduced. The leg offset voltage is used to regulate the circulating current and has little effect on ac and dc terminal voltages. The conventional balancing controls need the circulating current controller that produces the leg offset voltage reference from the input of circulating current references using the proportional

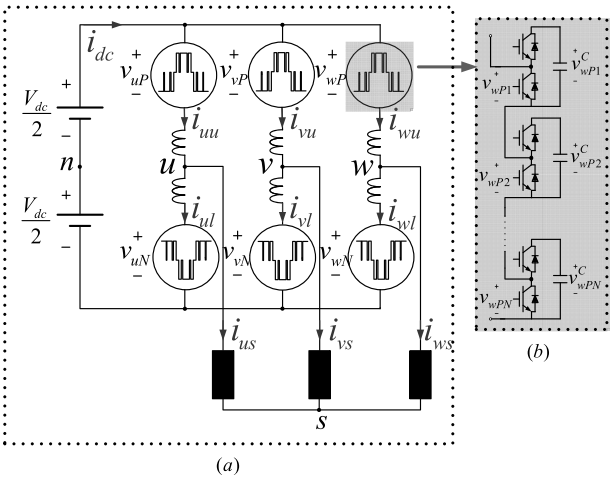

Fig. 1. Circuit configuration of the MMC.

and integral (PI) or the proportional and resonant controller. The performance of the circulating current controller has detrimental effects on the dynamics and complexity of the balancing control. Therefore, to improve the balancing performance by increasing bandwidth of the balancing controller, this paper proposes a balancing control method without the circulating current controller. Therefore, in the view point of capacitor voltage balancing, the leg offset voltage can be directly obtained with no phase delay due to the circulating current controller. Therefore, the bandwidth of balancing controller based on the direct voltage injection method can be extended more than that based on the circulating current controller. In addition, the difference between the cell voltages can be reduced faster. As a result, from the perspective of the control dynamics and control complexity, the proposed leg offset voltage injection method is better and simpler than the conventional circulating current injection method. Furthermore, the injecting frequency of leg offset voltage injection method can be increased more than that of current injection method, because of the extended bandwidth of the proposed method. Therefore, owing to the high-frequency injection with the proposed method, the fluctuation of cell capacitor voltage can be minimized compared with circulating current injection method.

The goal of this paper is to propose a control strategy of the entire frequency range operation including standstill for variable speed ac motor drive. The proposed method reduces the control performance degradation of the MMC when the load torque abruptlychanges. The control scheme introduces two operation modes: 1) a low-frequency mode for start-up and low-speed operation and 2) a normal frequency mode from medium to higher speed operation. The strategy in the low-frequency mode exploits leg offset voltage and common mode voltage with the high-frequency component to suppress the cell capacitor voltage ripple. The square wave voltage is used as the leg offset voltage, which shows that the circulating current peak is reduced when compared with sinusoidal waveform of the voltage [7]. A switchover tactic between two operation modes is described to drive the ac machine in the overall speed region.

To prove the effectiveness of the proposed control strategies, a 12-kV 24-MVA MMC-based adjustable motor drive system was designed using the PSIM software. The simulation results could offer the feasibility and advantage of the devised method for high-power medium voltage drives with MMC. In addition, experiments for variable-speed ac motor drives by a 10-kVA prototype MMC emulating fans, blowers, or pump drive system were performed to verify the feasibility of the proposed balancing strategy. The experiments were conducted for comparing features of the sinusoidal and square wave leg offset voltage. The stable operation at 1 Hz, which is <2% of the rated speed, is shown under an abrupt step load torque disturbance from 0% to 40% to demonstrate the dynamic performance. The experimental results show that all control strategies was well incorporated in the variable-speed ac motor drive system with a load where the torque varies in proportional to the square of the speed, like fans, blowers, or pumps.

II. Configuration and Basic Principle of the MMC

Fig. 1(a) shows the circuit configuration of the MMC. The three-phase MMC is composed of three legs and each leg has two arms and two arm inductors. Each arm has cascaded N-identical half-bridge circuit-based cells, and each cell consists of one dc capacitor and two active switching devices. The cascaded cell modules are shown in Fig. 1(b) in detail. In Fig. 1(a), i_{xu} and i_{xl} are the upper and lower arm currents, respectively, and i_{xs} is the output phase current where x' represents the u-, v-, or w-phase. The output phase current, i_{xs}, and circulating current, i_{xo}, are calculated from the upper and lower arm currents described in (1) and (2). Therefore, the arm currents can be deduced as (3) and (4), according to the decoupled control scheme in [8] and [11]

$$i_{\mathrm{xs}} = i_{\mathrm{xu}} - i_{\mathrm{xl}} \tag{1}$$

$$i_{\mathrm{xo}} = \frac{(i_{\mathrm{xu}} + i_{\mathrm{xl}})}{2} \tag{2}$$

$$i_{\mathrm{xu}} = \frac{1}{2} i_{\mathrm{xs}} + i_{\mathrm{xo}} \tag{3}$$

$$i_{\mathrm{xl}} = -\frac{1}{2} i_{\mathrm{xs}} + i_{\mathrm{xo}}. \tag{4}$$

The leg offset voltage, υ_{xo}, produces a circulating current defined as (5), where R and L stand for the resistance and inductance of an arm inductor when all arm inductors in MMC are assumed to be identical. From the voltage relationships along the x-phase loop, the upper, and lower arm voltage references are denoted as (6) and (7), respectively, where V_{dc} is the dc-link voltage, and υ_{xP} and υ_{xN} are the upper and lower arm voltages, respectively. The common mode voltage, υ_{sn}, is the voltage difference between nodes s' and n', and υ_{xs} is the phase voltage, which is $\upsilon_{\mathrm{xs}} = V_m \cos(\omega_s t)$. A detailed mathematical description of the relationships in an MMC is given in [10]

$$\upsilon_{\mathrm{xo}} = \left(R + L\frac{d}{\mathrm{dt}} \right) i_{\mathrm{xo}} \tag{5}$$

$$\upsilon^*_{\mathrm{xP}} = \frac{V_{\mathrm{dc}}}{2} - \upsilon^*_{\mathrm{xs}} - \upsilon^*_{\mathrm{sn}} - \upsilon^*_{\mathrm{xo}} \tag{6}$$

$$\upsilon^*_{\mathrm{xN}} = \frac{V_{\mathrm{dc}}}{2} + \upsilon^*_{\mathrm{xs}} + \upsilon^*_{\mathrm{sn}} - \upsilon^*_{\mathrm{xo}}. \tag{7}$$

The instantaneous power of each arm in the x-phase can be deduced as (8) and (9). These two equations must be considered to understand of the proposed balancing control

$$P_{\mathrm{xP}} = v_{\mathrm{xP}}^{*} i_{\mathrm{xu}} = \left(\frac{V_{\mathrm{dc}}}{2} - v_{\mathrm{xs}}^{*} - v_{\mathrm{sn}}^{*} - v_{\mathrm{xo}}^{*}\right)\left(\frac{1}{2} i_{\mathrm{xs}} + i_{\mathrm{xo}}\right) \tag{8}$$

$$P_{\mathrm{xN}} = v_{\mathrm{xN}}^{*} i_{\mathrm{xl}} = \left(\frac{V_{\mathrm{dc}}}{2} + v_{\mathrm{xs}}^{*} + v_{\mathrm{sn}}^{*} - v_{\mathrm{xo}}^{*}\right)\left(-\frac{1}{2} i_{\mathrm{xs}} + i_{\mathrm{xo}}\right). \tag{9}$$

In addition, the upper and lower arm energy can be calculated by (10) and (11), respectively. Each arm energy is the sum of the cell capacitor energies in the corresponding arm at x-phase leg

$$E_{\mathrm{xP}} = \frac{1}{2} C_{\mathrm{cell}} \sum_{i=1}^{N} \left(v_{\mathrm{xPi}}^{C}\right)^2 \tag{10}$$

$$E_{\mathrm{xN}} = \frac{1}{2} C_{\mathrm{cell}} \sum_{i=1}^{N} \left(v_{\mathrm{xNi}}^{C}\right)^2. \tag{11}$$

III. Proposed Balancing Control Scheme

A. Start-Up and Low Frequency Mode

The capacitor power difference between the upper and lower arm, which is derived as (12) from (8) and (9), affects the cell capacitor voltage balance of the arms. The first two terms on the right-hand side in (12), $0.5 V_{\mathrm{dc}} i_{\mathrm{xs}} - 2 v_{\mathrm{xs}}^{*} i_{\mathrm{xo}}$, have considerable dc or very low-frequency components. Thus, when the output frequency is dc or very low, the voltage difference between the arms will diverge due to this low-frequency term

$$P_{\mathrm{xP}} - P_{\mathrm{xN}} = 0.5 V_{\mathrm{dc}} i_{\mathrm{xs}} - 2 v_{\mathrm{xs}}^{*} i_{\mathrm{xo}} - 2 v_{\mathrm{sn}}^{*} i_{\mathrm{xo}} - v_{\mathrm{xo}}^{*} i_{\mathrm{xs}}. \tag{12}$$

To balance the power difference between arms, a control strategy exploiting the common mode voltage, v_{sn}, was used in this paper. The common mode voltage can be regarded as an additional degree of freedom for controllability since the common mode voltage does not affect the line-to-line output voltage. It is natural to select the frequency of the common mode voltage as a high frequency to minimize the cell capacitor voltage fluctuations. In addition, since the circulating current, i_{xo}, is also a controllable element that does not affect the output phase current, a high-frequency component can be superimposed on the circulating current. Hence, the third term on the right-hand side in (12), $2 v_{\mathrm{sn}}^{*} i_{\mathrm{xo}}$ can be used to balance the power of arms with the high-frequency components in v_{sn} and i_{xo}. For convenience, the low- and high-frequency elements can be segregated from i_{xo} and v_{sn} as (13) and (14), where ~ and ^ refer to the low and high-frequency components, respectively

$$i_{\mathrm{xo}} = \tilde{i}_{\mathrm{xo}} + \hat{i}_{\mathrm{xo}} \tag{13}$$

$$v_{\mathrm{sn}} = \hat{v}_{\mathrm{sn}}. \tag{14}$$

The power difference between the upper and lower arms can be rearranged from (12) to (14), and then, the low-frequency power component can be extracted as in (15). Here, the power difference should be controlled as null

$$\begin{aligned}(P_{\mathrm{xP}} - P_{\mathrm{xN}})|_{\text{low freq.}} &\approx 0.5 V_{\mathrm{dc}} i_{\mathrm{xs}} - 2 v_{\mathrm{xs}}^{*} \tilde{i}_{\mathrm{xo}} - 2 \hat{v}_{\mathrm{sn}}^{*} \hat{i}_{\mathrm{xo}}^{*}\Big|_{\text{low freq.}} = 0. \end{aligned} \tag{15}$$

To nullify the low-frequency component as in (15), the low-frequency component of $2 \hat{v}_{\mathrm{sn}}^{*} \hat{i}_{\mathrm{xo}}^{*}$ should be controlled. Thus, $\hat{v}_{\mathrm{sn}}^{*}$ and $\hat{i}_{\mathrm{xo}}^{*}$ should be regulated as the same high-frequency, to make the power term of $2 \hat{v}_{\mathrm{sn}}^{*} \hat{i}_{\mathrm{xo}}^{*}$ have dc or low-frequency component.

In the case of the sinusoidal leg offset voltage injection method, $\hat{v}_{\mathrm{sn}}^{*}$ and $\hat{v}_{\mathrm{xo}}^{*}$ can be defined as (16) and (17), and ω_h refers to the angular speed of the high-frequency component, V_{sn} for the effective value of common mode voltage, and $\tilde{V}_{\mathrm{xo}}$ for the magnitude of high-frequency leg offset voltage, which may have dc and several low-frequency components

$$\hat{v}_{\mathrm{sn}}^{*} = \sqrt{2} V_{\mathrm{sn}} \cos(\omega_h t) \tag{16}$$

$$\hat{v}_{\mathrm{xo}}^{*} = \tilde{V}_{\mathrm{xo}} \cos(\omega_h t + \phi). \tag{17}$$

The phase angle ϕ in (17) between the leg offset voltage and circulating current is derived from (18) to make the circulating current synchronize with the common mode voltage

$$\phi = \arctan\left(\frac{\omega_h L}{R}\right). \tag{18}$$

In general, $\omega_h L$ is much larger than R, because the frequency of injecting voltage is quite high. However, if the frequency is not high enough and the arm resistance cannot be ignored, the arm impedance parameters would need to be identified. For identification, at the system commissioning stage, the noninteracting leg offset voltage can be injected into the arm, and the circulating current could befed back as in (5). Consequently, the phase angle between the leg offset voltage and the circulating current in (18) can be obtained. Under the assumption of $R \ll \omega_h L$, ϕ is approximately $\pi/2$. From (5), (16) and (17), the low-frequency component of the power associated with the common mode voltage and the circulating current can be derived as (19) using the leg offset voltage, where p represents a differential operator

$$\begin{aligned} 2 \hat{v}_{\mathrm{sn}} \hat{i}_{\mathrm{xo}}\Big|_{\text{low freq.}} &\approx 2 \hat{v}_{\mathrm{sn}} \frac{\hat{v}_{\mathrm{xo}}}{pL}\Big|_{\text{low freq.}} \\ &= \frac{2\sqrt{2} V_{\mathrm{sn}} \tilde{V}_{\mathrm{xo}}}{\omega_h \mathrm{L}} \cos(\omega_h t) \sin\left(\omega_h t + \frac{\pi}{2}\right)\Big|_{\text{low freq.}} \\ &= \frac{2\sqrt{2} V_{\mathrm{sn}} \tilde{V}_{\mathrm{xo}}}{\omega_h \mathrm{L}} \left(\frac{1}{2}\sin\left(\frac{\pi}{2}\right) + \frac{1}{2}\sin\left(2\omega_h t + \frac{\pi}{2}\right)\right)\Big|_{\text{low freq.}} \\ &= \frac{\sqrt{2} V_{\mathrm{sn}} \tilde{V}_{\mathrm{xo}}}{\omega_h \mathrm{L}}. \end{aligned} \tag{19}$$

And then, $2 \hat{v}_{\mathrm{sn}}^{*} \hat{i}_{\mathrm{xo}}^{*}$ in (15) can be substituted with (19). The magnitude of high-frequency leg offset voltage, $\tilde{V}_{\mathrm{xo}}$, can be calculated as

$$\begin{aligned} \frac{\sqrt{2} V_{\mathrm{sn}} \tilde{V}_{\mathrm{xo}}}{\omega_h \mathrm{L}} &\approx \frac{1}{2} V_{\mathrm{dc}} i_{\mathrm{xs}} - 2 v_{\mathrm{xs}}^{*} \tilde{i}_{\mathrm{xo}} \\ \tilde{V}_{\mathrm{xo}} &\approx \frac{\omega_h \mathrm{L}}{\sqrt{2} V_{\mathrm{sn}}} \left(\frac{1}{2} V_{\mathrm{dc}} i_{\mathrm{xs}} - 2 v_{\mathrm{xs}}^{*} \tilde{i}_{\mathrm{xo}}\right). \end{aligned} \tag{20}$$

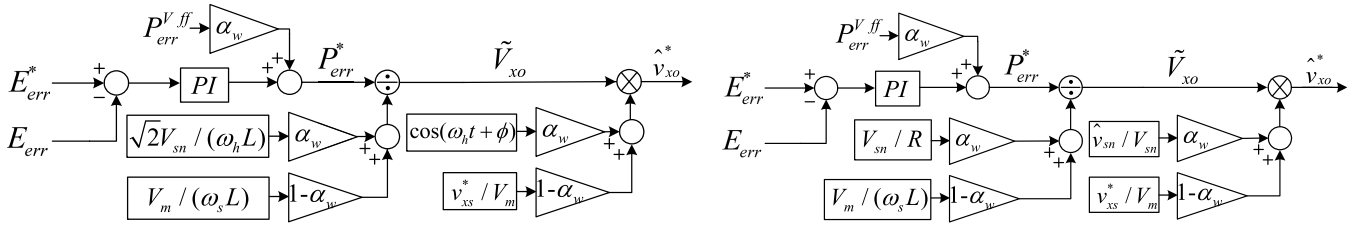

Fig. 2. Proposed control scheme for variable-speed drives. (a) Sinusoidal wave voltage injection method. (b) Square wave voltage injection method. α_W is weighting factor for switchover, which is described in Section III-C.

In the case that the sinusoidal wave voltage is injected to both the common mode and the leg offset voltage, the balancing control strategy is shown as a block diagram in Fig. 2(a). $E_{\rm err}$ is the energy difference between the upper and lower arms as in (21). $E_{\rm err}^*$ is the reference of energy difference and should be set as null to keep the balance of the arm energies

$$E_{\rm err} = E_{\rm xP} - E_{\rm xN} = \frac{1}{2} C_{\rm cell} \left\{ \sum_{i=1}^{N} \left(v_{\rm xPi}^C \right)^2 - \sum_{i=1}^{N} \left(v_{\rm xNi}^C \right)^2 \right\}. \tag{21}$$

$P_{\rm err}^{\rm Vff}$ in Fig. 2(a) can be derived as (22) by (20)

$$P_{\rm err}^{\rm Vff} = \frac{1}{2} V_{\rm dc} i_{\rm xs} - 2 v_{\rm xs}^* \tilde{i}_{\rm xo}. \tag{22}$$

In the case of the square leg offset voltage injection, on the other hand, the square wave voltage can be injected to both the common mode and the leg offset voltage as shown in Fig. 2(b). In this case, $\hat{v}_{sn}^*$ can be defined by (23) and f_h stands for the frequency of the injected high-frequency voltage

$$\hat{v}_{\rm sn}^* = \begin{cases} -V_{\rm sn} & \left(0 \le t < \frac{1}{2f_h}\right) \\ V_{\rm sn} & \left(\frac{1}{2f_h} \le t < \frac{1}{f_h}\right). \end{cases} \tag{23}$$

Under the assumption that the arm resistance, R, is dominant during each given quasisteady half period, $1/(2f_h)$, $\hat{v}_{\rm xo}^*$ can be approximated as (24) from (5), (15), and (23)

$$\hat{v}_{\rm xo}^* \approx \begin{cases} -\frac{R}{2V_{\rm sn}} \left(\frac{1}{2} V_{\rm dc} i_{\rm xs} - 2 v_{\rm xs}^* \tilde{i}_{\rm xo} \right) & \left(0 \le t < \frac{1}{2f_h}\right) \\ \frac{R}{2V_{\rm sn}} \left(\frac{1}{2} V_{\rm dc} i_{\rm xs} - 2 v_{\rm xs}^* \tilde{i}_{\rm xo} \right) & \left(\frac{1}{2f_h} \le t < \frac{1}{f_h}\right). \end{cases} \tag{24}$$

$P_{\rm err}^{\rm Vff}$ in Fig. 2(b) can also be derived from (22) using (24) similarly with the case of sinusoidal wave.

B. Normal Frequency Mode

Since the output frequency is high enough in the normal frequency mode, the voltage fluctuation of the cell capacitor is tolerable. In this mode, the circulating current is controlled to have only dc component to minimize the conduction loss caused by the additional circulating current. As the operation frequency increases, meanwhile, the margin of the common mode voltage decreases. Hence, the common mode voltage is less available for balancing control.

Practical MMC systems may have an inherent unbalance due to slight asymmetries in cells, structural errors, and other issues. In normal frequency mode, therefore, it should be performed just to eliminate the inevitable small dc unbalances. The balancing can be achieved using the circulating current as $2v_{\rm xs}^* i_{\rm xo}$ in (12). By regulating the leg offset voltage for circulating current to have fundamental frequency component, this dc unbalance can be suppressed.

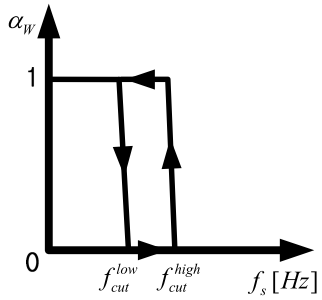

Fig. 3. Relationship between operating frequency and weighting factor.

C. Switchover Between Two Modes

As mentioned previously, as the high-frequency components of the common mode and leg offset voltage are only injected in low-operating frequency modes, the leg offset voltage reference changes depending on the output frequency of MMC. A switchover tactic between the low- and high-frequency modes shown in Fig. 3 is devised by the weighting factor, α_W. In addition, this factor is applied to the switchover of the balancing control scheme shown in Fig. 2. In addition, the tactic would have the hysteresis band to prevent chattering in the vicinity of the switchover frequency, $f_{\rm cut}$.

IV. Overall Control Scheme for Entire Frequency Operation

Fig. 4 shows the overall controller for the entire frequency operation from standstill to normal frequency mode. First, the averaging controller carries out regulating the leg power, which is the difference between dc-link input power and ac output power. The leg power is calculated as (25) by adding (8) and (9)

$$P_{\rm xP} + P_{\rm xN} \approx V_{\rm dc} \tilde{i}_{\rm xo} - 2 v_{\rm xo}^* \hat{i}_{\rm xo} - v_{\rm xs}^* i_{\rm xs} - \hat{v}_{\rm sn}^* i_{\rm xs}. \tag{25}$$

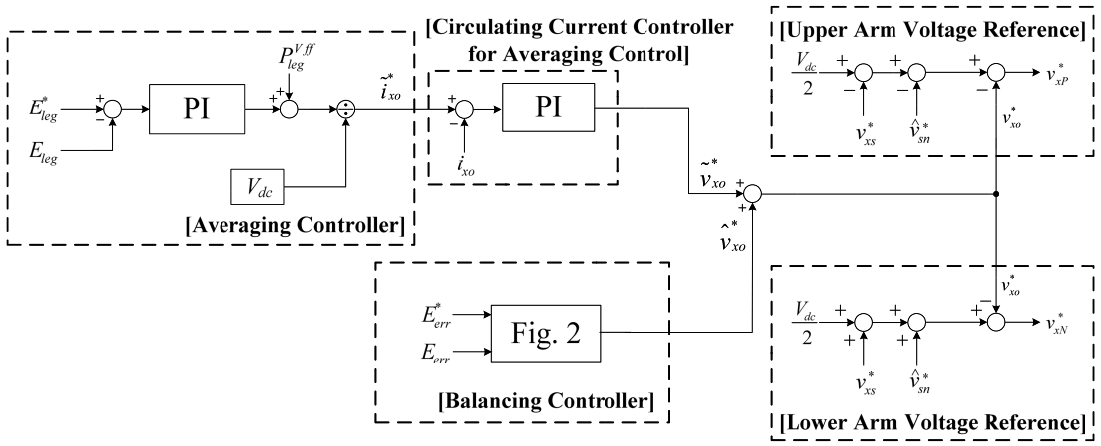

Fig. 4. Proposed overall control scheme for variable-speed drives.

Because the low-frequency power component in (25) should be nullified as in (26), the controller output has dc and second-order harmonic frequency components as described in (27)

$$P_{\mathrm{xP}} + P_{\mathrm{xN}}|_{\text{low freq.}} \approx V_{\mathrm{dc}}\tilde{i}^{*}_{\mathrm{xo}} - v^{*}_{\mathrm{xs}} i_{\mathrm{xs}} = 0 \tag{26}$$

$$\tilde{i}^{*}_{\mathrm{xo}} = v^{*}_{\mathrm{xs}} i_{\mathrm{xs}} / V_{\mathrm{dc}}. \tag{27}$$

E_{leg} is the energy of the leg and it can be calculated as (28). E^{*}_{leg} is the reference energy of the leg as (29), where v^{*}_{c} is the reference value of cell capacitor voltage, V_{dc}/N

$$E_{\mathrm{leg}} = E_{\mathrm{xP}} + E_{\mathrm{xN}} = \frac{1}{2} C_{\mathrm{cell}} \left\{ \sum_{i=1}^{N} \left(v^{C}_{\mathrm{xPi}} \right)^2 + \sum_{i=1}^{N} \left(v^{C}_{\mathrm{xNi}} \right)^2 \right\} \tag{28}$$

$$E^{*}_{\mathrm{leg}} = \frac{1}{2} \frac{C_{\mathrm{cell}}}{2N} 4N^2 v^{*2}_{c} = N C_{\mathrm{cell}} v^{*2}_{c}. \tag{29}$$

The feed-forwarding power term, $P^{\mathrm{V\,ff}}_{\mathrm{leg}}$, can be derived as $v^{*}_{\mathrm{xs}} i_{\mathrm{xs}}$ from (27). Therefore, the PI controller can simply be adopted as the circulating current controller for the averaging control. The details about the averaging controller are described in [10].

Meanwhile, the balancing controller can be chosen between two schemes in Fig. 2 that are namely, the sinusoidal and the square wave voltage injections. As shown in Fig. 4, the balancing controller directly makes the leg offset voltage without the circulating current controller to eliminate the energy difference between upper and lower arms. By reason of this fact, the balancing controller has a wider bandwidth, and can achieve a better transient response compared with the control scheme based on the inner circulating current regulation loop.

Finally, the upper and lower arm voltage references are synthesized as (6) and (7), which are composed of v^{*}_{xs} from the output of phase current controller, v^{*}_{xo} from the averaging and balancing controller, and the injected common mode voltage of $\hat{v}^{*}_{\mathrm{sn}}$.

V. Simulation Results

To verify the effectiveness of the proposed control strategy, an adjustable speed drive system based on 12-kV 24-MVA MMC has been implemented using the time-domain simulation program, PSIM. The number of cells in each arm, N, equals 20. Thus, the system with 120 cells was simulated. Each cell capacitor voltage is controlled as 600 V, and the cell is composed of the half-bridge inverter and the cell capacitance is 6000 μF. The nearest level modulation is applied to generate the arm voltage references and reduce the switching loss of MMC [15]. The cell voltage sorting algorithm is applied to the cell voltage balancing [14]. The parameters used in the simulation are listed in Table I.

TABLE I
Circuit Parameters of the Simulations

Description	Abbreviation	Value
Rated apparent power	S_{MMC}	24MVA
Rated line-to-line rms voltage	V_S	8.32kV
Rated line frequency	f_S	60Hz
DC-link voltage	V_{dc}	12kV
Cell capacitance	C_{cell}	6000μF
Arm inductance	L	4mH

TABLE II
PMSM Specification of the Simulations

Description	Abbreviation	Value
Rated active power	P_{PMSM}	20MW
Rated line-to-line rms voltage	V_{rated}	8kV
Rated rotational speed	ω^{rated}_{rm}	360r/min
Pole pair number	pp	10

It is assumed that the 21-level MMC system drives a 20 MW 20-pole permanent magnet synchronous machine (PMSM) with adjustable mechanical load. The PMSM parameters are summarized in Table II.

From the simulation results the devised method can be applied to high-power medium voltage adjustable drive system

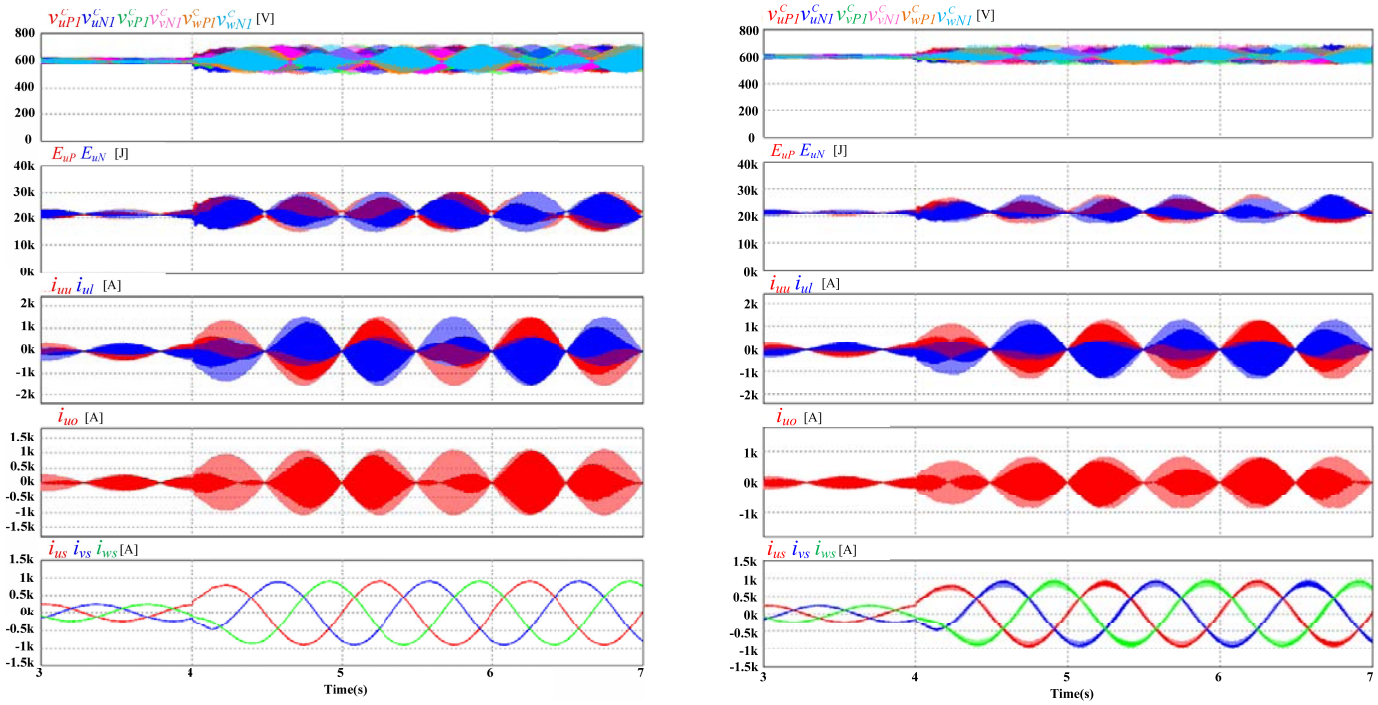

Fig. 5. Simulation waveform when applying the proposed leg offset voltage injection method with 6r/min speed and step load torque from 10% to 40% of the rated torque. (a) Sinusoidal waveform offset voltage injection. (b) Square waveform offset voltage injection.

based on MMC. From the dynamic comparison between circulating current injection with the inner current loop and the proposed leg offset voltage injection method, it can be concluded that the proposed method might be an acceptable solution for high-power medium voltage drives based on MMC under requirements of considerable torque disturbance and steady state operation down to a few percent of rated frequency.

Fig. 5 shows the low-frequency operation at 1 Hz (6 r/min, <2% of the rated frequency) with an abrupt step load torque from 50 kN · m (10%) to 200 kN · m (40%) at 4 s. Fig. 5(a) shows the simulation result of the sinusoidal wave leg offset voltage method, and Fig. 5(b) shows that of the square wave leg offset voltage method. The high-frequency (100 Hz) voltage is used to balance the arm in low the frequency mode in both sinusoidal and square wave cases. Before 4 s, the PMSM is controlled to be 6 r/min with 10% load torque. At the time point 4 s, the 40% load torque is abruptly applied to the PMSM. Regardless of the impact of step load torque, MMC systems with both sinusoidal and square wave cases have successfully kept the stable operation. Meanwhile, comparing the waveforms between Fig. 5(a) and (b), the square waveform method can save the magnitude of the circulating current. In addition, it has better balancing ability than the sinusoidal waveform method, from the view of the u-phase upper and lower cell capacitor voltage fluctuations.

Meanwhile, in Fig. 6, the simulation results with the conventional circulating current injection method based on the inner current regulating loop is shown. All operating conditions are identical to those in Fig. 5 except for the magnitude of the step load torque. For fair comparison between the conventional current injection and proposed leg offset voltage injection methods, the bandwidth for the balancing controller of the

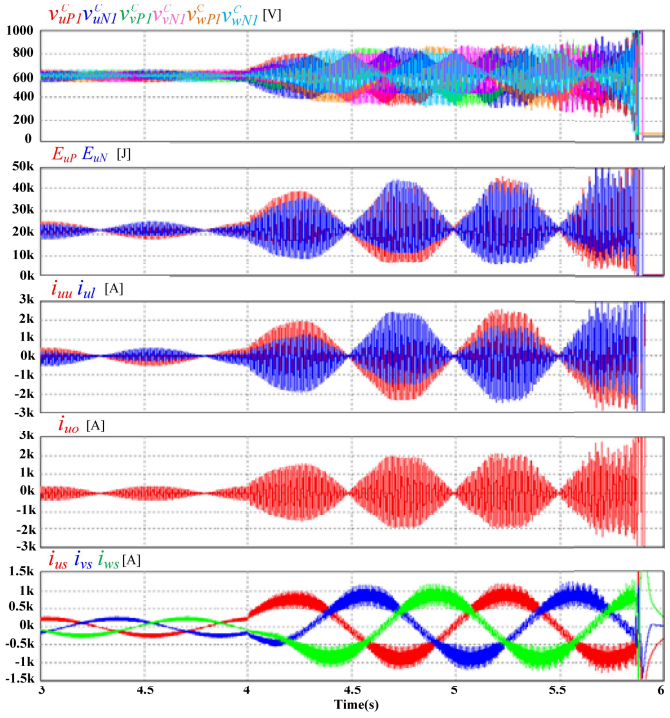

Fig. 6. Simulation waveform when applying the conventional circulating current injection method with 6 r/min speed and step load torque from 10% to 36% of the rated torque.

two methods is set as the same, and the frequency of the injected component was also set as the same, 100 Hz. The magnitude of the step load torque applied at the conventional current injection method is 36% of the rated torque, which

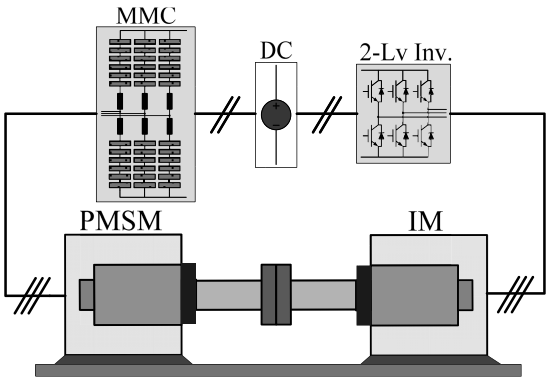

Fig. 7. Experimental setup with 300 V 10 kVA prototype MMC system.

TABLE III
CIRCUIT PARAMETERS OF THE EXPERIMENTS

Description	Abbreviation	Value
Rated active power	P_{PMSM}	11kW
Rated line-to-line rms voltage	V_{rated}	200V
Rated rms line current	I_{rated}	58.6A
Rated rotational speed	ω_{rm}^{rated}	1750r/min
Pole pair number	pp	4

TABLE IV
PMSM SPECIFICATION OF THE EXPERIMENTS

Description	Abbreviation	Value
Rated active power	P_{PMSM}	11kW
Rated line-to-line rms voltage	V_{rated}	200V
Rated rms line current	I_{rated}	58.6A
Rated rotational speed	ω_{rm}^{rated}	1750r/min
Pole pair number	pp	4

is less than the proposed method test in Fig. 5. As shown in Fig. 6, the system based on the conventional method becomes unstable and stalls in a moment at the end. After the abrupt step load torque is applied at 4 s, the cell capacitor voltage fluctuations are larger than the fluctuations when using the leg offset voltage injection method in Fig. 5.

VI. EXPERIMENTAL RESULTS

The proposed control strategy is validated by the 300 V 10 kVA reduced scale prototype MMC shown in Fig. 7. The number of cells in each arm, N, is 6, so there are a total of 36 cells used for the three-phase system. Each cell capacitor voltage is controlled at 50 V and each cell includes two power MOSFET switches, which have 100 V/120-A ratings. The level-shifted phase disposition pulsewidth modulation generates arm voltage references [12], [13], and the voltage balancing of cell capacitors in each arm is achieved by sorting algorithms [14]. The carrier frequency of each cell is set as

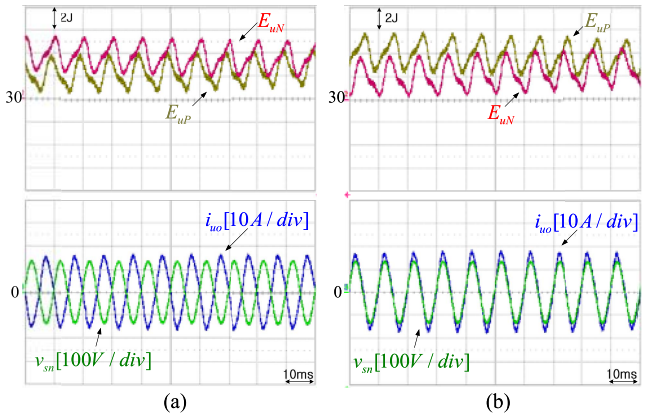

Fig. 8. Experimental waveform of the low frequency mode operation at 1 Hz output frequency with the sinusoidal leg offset voltage. (a) Negative energy difference. (b) Positive energy difference.

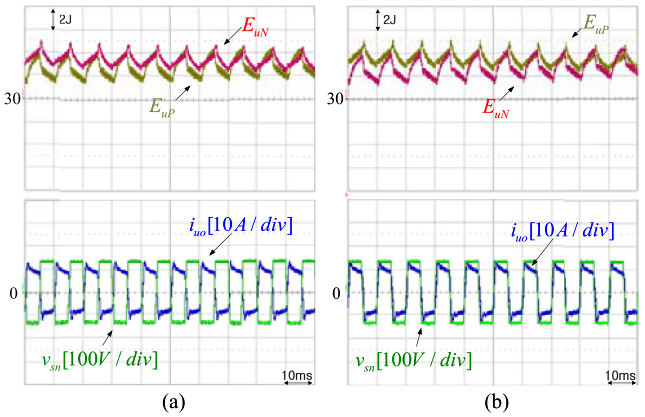

Fig. 9. Experimental waveform of the low frequency mode with 1 Hz output frequency when using the square leg offset voltage. (a) Negative energy difference. (b) Positive energy difference.

2 kHz and the dc link capacitance of each cell is 4400 μF. The parameters of the system under test are summarized in Table III.

The MMC is connected to drive 11-kW 8-pole PMSM coupled to an induction machine (IM) for applying load torque to PMSM, as shown in Fig. 7. The rated torque and speed of the PMSM are 60 N · m and 1750 r/min, respectively. The PMSM specifications are summarized in Table IV.

A. Sinusoidal Leg Offset Voltage Injection

Fig. 8 shows the waveform in condition of the low-frequency operation mode at 1-Hz output frequency with 20% load torque. The injected leg offset voltage is the 100-Hz sinusoidal wave. Fig. 6 shows the upper and lower arm energy of the u-phase calculated from (10) to (11). The difference between the upper and lower arm is counter balanced by $\hat{v}_{\mathrm{sn}}^{*}\hat{i}_{\mathrm{xo}}^{*}$. When the energy difference, E_{uP}-E_{uN}, is negative, the high-frequency circulating current and offset voltage are controlled 180° out of phase, as shown in Fig. 8(a). In contrast, when the difference is positive, the circulating current and offset voltages are controlled to be in phase in Fig. 8(b).

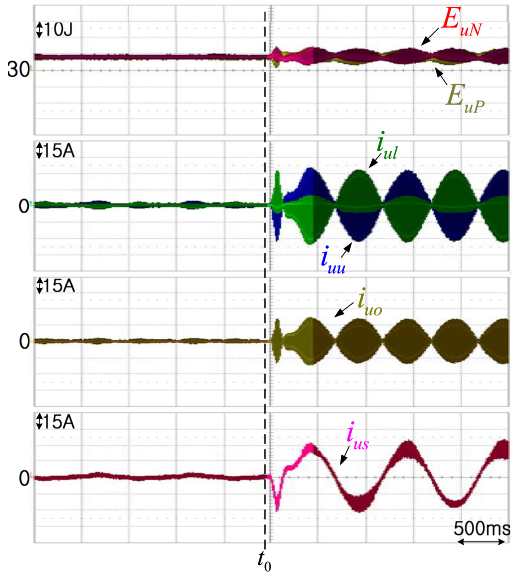

Fig. 10. Experimental waveform when applying the leg offset voltage injecion method with $\omega_{\mathrm{rm}} = 15$ r/min and 40% step load torque at t_0.

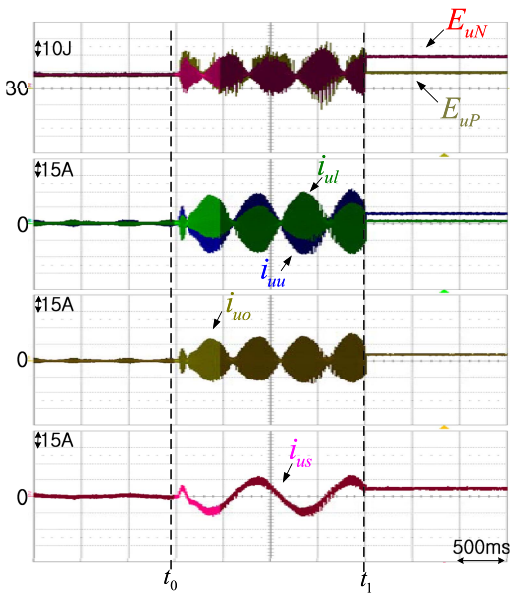

Fig. 11. Experimental waveform when applying the conventional circulating current injecion method with $\omega_{\mathrm{rm}} = 15$ r/min and 20% step load torque at t_0.

B. Square Leg Offset Voltage Injection

Fig. 9 is the waveform of the low-frequency operation mode at 1-Hz output frequency with 20% load torque. The balancing control is performed using the 100-Hz square wave leg offset voltage. Fig. 9 shows the energy of the upper and lower arm in the u-phase leg. The energy difference is counter balanced by $v^*_{\mathrm{sn}} i_{\mathrm{xo}}$ as in the preceding sinusoidal wave case. In this experiment, the trapezoidal wave was used instead of square wave, because the output voltage might have unwanted high-frequency distortion due to the nonlinearities of cells, such as dead time. If the energy difference, E_{uP}-E_{uN}, is negative, the high-frequency circulating current and offset voltage are controlled to be 180° out of phase, as shown in Fig. 9(a). In contrast, when the difference is positive, the circulating current and offset voltages are controlled to be in phase, as in Fig. 9(b).

As described in [7], the square wave can shave the peak of circulating current by 50%. However, because of trapezoidal waveform in this experiment the peak value of circulating current (i_{xo}) is smaller by 37% than that of the sinusoidal voltage case.

C. Dynamic Comparison Between Circulating Current Injection and Leg Offset Voltage Injection

Fig. 10 shows the low-frequency operation at 1 Hz (15 r/min, <2% of the rated speed) when an abrupt step load torque was applied from 0 to 24 N•m (40%) at t_0. The square wave leg offset voltage is injected in 100 Hz for the arm balancing at this experimental result. Before time point, t_0, the PMSM was controlled to be 15 r/min without load torque. At the time point, t_0, the 40% step load torque is applied through torque control of the IM. After t_0, the upper and lower arm energy fluctuations became larger because of the significant output phase current by the step load torque. Furthermore, the transient response in the circulating current becomes well regulated within 300 ms after the step variation in the torque. Regardless of the impact of load torque, PMSM has successfully kept the speed showing reasonable low-speed performance. This result confirms that the proposed controller achieves a good transient response.

In contrast, the conventional circulating current injection method with the inner current regulating loop has been applied to balancing control, as shown in Fig. 11. For fair comparison between the conventional current injection and the proposed leg offset voltage injection methods, the bandwidth for two methods was set as the same, and the frequency of the injected component was also set as the same, 100 Hz. However, the magnitude of the step load torque applied at the conventional current injection method was half of the proposed method in Fig. 10. As shown in Fig. 11, the system became unstable and stalled at the end despite the lower external load torque. After the abrupt step load torque was applied at t_0, the fluctuations of the upper and lower arm energies were larger than that when using leg offset voltage injection method in Fig. 10. Finally, the balancing controller could not achieve system balance, and the overvoltage trip of cell capacitor occurredand the system stalled at the time point of t_1.

And it can be concluded that the leg offset voltage injection method has better disturbance load torque rejection performance.

D. Operation from Standstill to Normal Frequency Mode

Finally, Fig. 12 shows the entire operation from standstill to the normal frequency mode, 1000 r/min. To conduct the switchover operation in a practical application of variable speed drive, such as fans, blowers, or pumps, the load torque was emulated with IM in proportional to the square of the speed. Furthermore, the start-up torque of 24 N · m (40%) is included in the torque profile ($T_{\mathrm{L\_profile}}$). In addition, the phase current before t_{start} is regulated as the dc value. At the time point t_{change}, the switchover process starts, and the operating

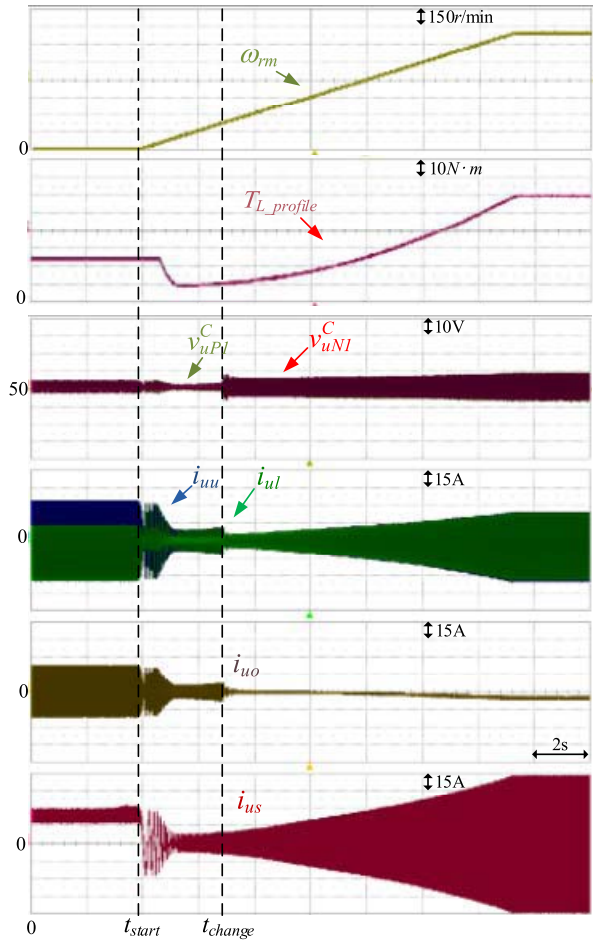

Fig. 12. Experimental waveforms in the condition of variable speed drive from starting to 1000 r/min with 40% starting torque and the increasing load torque depending on rotating speed.

mode changes to the normal frequency operation mode. When the rotating speed ($\omega_{\rm rm}$) is 1000 r/min, the applied load torque to PMSM is 100% of the rated torque, 60 N · m. As shown in Fig. 12, it has been confirmed that the proposed control strategies shown in Fig. 4 are well implemented and incorporated properly to drive the variable speed ac machine in overall speed including standstill by the MMC.

VII. Conclusion

In this paper, a control strategy for variable-speed ac motor drives based on MMC has been presented. To overcome the difficulties of the power balance between cells and arms of MMC over wide operation speed ranges, a direct leg offset voltage injection method has been devised. Utilizing the proposed method, the ripple voltage of each cell of MMC has been kept within allowable bounds under the sudden application of 40% of rated load torque at the extremely low frequency, 1 Hz, which is <2% of rated frequency. Based on the simulation and experimental results, it can be noted that the control performance of the upper and lower arm energy ripple by the proposed leg offset voltage injection method is better than that by the conventional circulating current injection method with the inner loop. In addition, the variable speed ac motor drive has been proven to work based on the switchover tactic by testing the overall speed including standstill.

References

[1] A. Lesnicar and R. Marquardt, "An innovative modular multilevel converter topology suitable for a wide power range," in *Proc. IEEE Power Tech Conf.*, Bologna, Italy, Jun. 2003.

[2] M. Hiller, D. Krug, R. Sommer, and S. Rohner, "A new highly modular medium voltage converter topology for industrial drive applications," in *Proc. 13th Eur. Conf. Power Electron. Appl.*, Sep. 2009. pp. 1–10.

[3] G. P. Adam, O. Anaya-Lara, G. M. Burt, D. Telford, B. W. Williams, and J. R. McDonald, "Modular multilevel inverter: Pulse width modulation and capacitor balancing technique," *IET Power Electron.*, vol. 3, no. 5, pp. 702–715, Sep. 2010.

[4] H. M. Pirouz, M. T. Bina, and K. Kanzi, "A new approach to the modulation and DC-link balancing strategy of modular multilevel AC/AC converters," in *Proc. Int. Conf. PEDS*, 2005, vol. 2, pp. 1503–1507.

[5] A. Antonopoulos, K. Ilves, L. Angquist, and H.-P. Nee, "On interaction between internal converter dynamics and current control of high-performance high-power AC motor drives with modular multilevel converters," in *Proc. IEEE ECCE*, Sep. 2010, pp. 4293–4298.

[6] M. Hagiwara, K. Nishimura, and H. Akagi, "A medium-voltage motor drive with a modular multilevel PWM inverter," *IEEE Trans. Power Electron.*, vol. 25, no. 7, pp. 1786–1799, Jul. 2010.

[7] M. Hagiwara, I. Hasegawa, and H. Akagi, "Start-up and low-speed operation of an electric motor driven by a modular multilevel cascade inverter," *IEEE Trans. Ind. Appl.*, vol. 49, no. 4, pp. 1556–1565, Jul./Aug. 2013.

[8] J. Kolb, F. Kammerer, and M. Braun, "Straight forward vector control of the modular multilevel converter for feeding three-phase machines over their complete frequency range," in *Proc. 37th Annu. Conf. IEEE Ind. Electron. Soc. IECON*, Nov. 2011, pp. 1596–1601.

[9] A. Antonopoulos, L. Angquist, S. Norrga, K. Ilves, and H.-P. Nee, "Modular multilevel converter AC motor drives with constant torque form zero to nominal speed," in *Proc. IEEE ECCE*, Sep. 2012, pp. 739–746.

[10] J.-J. Jung, H.-J. Lee, and S.-K. Sul, "Control of the modular multilevel converter for variable-speed drives," in *Proc. IEEE Int. Conf. PEDES*, Dec. 2012, pp. 1–6.

[11] L. Angquist, A. Antonopoulos, D. Siemaszko, K. Ilves, M. Vasiladiotis, and H.-P. Nee, "Inner control of modular multilevel converters-an approach using open-loop estimation of stored energy," in *Proc. IPEC*, Jun. 2010, pp. 1579–1585.

[12] T. Wang and Y. Zhu, "Analysis and comparison of multicarrier PWM schemes applied in H-bridge cascaded multi-level inverters," in *Proc. 5th ICIEA*, Jun. 2010, pp. 1379–1383.

[13] S. Rohner, S. Bernet, M. Hiller, and R. Sommer, "Modulation, losses, and semiconductor requirements of modular multilevel converters," *IEEE Trans. Ind. Electron.*, vol. 57, no. 8, pp. 2633–2642, Aug. 2010.

[14] X. Shi, Z. Wang, L. M. Tolbert, and F. Wang, "A comparison of phase disposition and phase shift PWM strategies for modular multilevel converters," in *Proc. IEEE ECCE*, Sep. 2013, pp. 4089–4096.

[15] M. Perez, J. Rodriguez, J. Pontt, and S. Kouro, "Power distribution in hybrid multi-cell converter with nearest level modulation," in *Proc. IEEE ISIE*, Jun. 2007, pp. 736–741.

[16] A. J. Korn, M. Winkelnkemper, and P. Steimer, "Low output frequency operation of the modular multi-level converter," in *Proc. IEEE ECCE*, Sep. 2010, pp. 3993–3997.

Jae-Jung Jung (S'13) was born in Korea in 1985. He received the B.S. and M.S. degrees in electrical engineering from Seoul National University, Seoul, Korea, in 2011 and 2013, respectively, where he is currently pursuing the Ph.D. degree in electrical engineering and computer science.

He was involved in sensorless converter and modular multilevel converter for motor drives. His current research interests include high-power conversion system, in particular, for VSC-HVDC.

Hak-Jun Lee (S'11) was born in Korea in 1980. He received the B.S., M.S., and Ph.D. degrees in electrical engineering from Seoul National University, Seoul, Korea, in 2007, 2009, and 2013, respectively.

He has been with the Research and Development Center, LSIS Company, Ltd., Anyang, Korea, since 2013, where he is currently involved in the electric machine drive systems and the modular multilevel converter for HVDC system. His current research interests include electric machine drive system, high-power converter, and multilevel converter.

Seung-Ki Sul (S'78–M'80–SM'98–F'00) received the B.S., M.S., and Ph.D. degrees in electrical engineering from Seoul National University, Seoul, Korea, in 1980, 1983, and 1986, respectively.

He was an Associate Researcher with the Department of Electrical and Computer Engineering, University of Wisconsin, Madison, WI, USA, from 1986 to 1988. From 1988 to 1990, he was a Principal Research Engineer with Gold-Star Industrial Systems Company, Seoul. Since 1991, he has been a Faculty Member with the School of Electrical Engineering, Seoul National University, where he is currently a Full Professor. From 2003 to 2004, he was a Research Director and an Acting Consultant with Yaskawa Electric Corporation, Fukuoka, Japan. From 2005 to 2007, he was the Vice Dean of the Engineering College, Seoul National University. From 2008 to 2011, he was the President of the Electrical Engineering Science Research Institute funded by the Korean Government. He has authored over 120 reviewed journal papers, in particular, the IEEE transactions. His current research interests include power electronic control of electrical machines, electric/hybrid vehicle and ship drives, and power-converter circuits for renewal energy sources.

Dr. Sul was a Technical Chair of the 2006 IEEE Power Electronics Specialists Conference and the General Chair of the 2011 IEEE Energy Conversion Congress and Exposition-Asia. He is currently the Editor-in-Chief of the *Journal of Power Electronics*, which is a SCIE registered journal, published by the Korean Power Electronics Institute, Seoul.